

Development of an attitude guidance and control system for the Thunderstar suborbital spacecraft

S C Greenland and W J Crowther*

School of Mechanical, Aerospace, and Civil Engineering, University of Manchester, Manchester, UK

The manuscript was received on 12 April 2006 and was accepted after revision for publication on 29 November 2006.

DOI: 10.1243/09544100JAERO106

Abstract: This paper outlines a method of developing a quaternion attitude guidance and control system for a rigid body suborbital spacecraft using cold gas thrusters over a short-duration mission. It has been specifically developed for integration aboard the Thunderstar spacecraft of Starchaser Industries, a three-man capsule designed for space tourism. The system described consists of three principal components: an autoflight computer that generates incidence and roll rate demands from analysis of the predicted flight path trajectory, a quaternion controller that produces a demand torque, and a pulse-width pulse-frequency modulator that determines the necessary thruster fire signals. The spacecraft attitude and flight path dynamics are defined within the upper to middle Earth atmosphere together with the cold gas thruster dynamics. The effect of disturbances on spacecraft attitude has been investigated and the most significant found to be due to crew motion and aerodynamics. The system concept has been evaluated through modelling in SIMULINK and has been found to meet the requirements laid out for a typical Thunderstar mission.

Keywords: quaternion, spacecraft, control system, architecture, suborbital, simulation, reaction control, cold gas thrusters

1 INTRODUCTION

Manned suborbital spaceflight has attained considerable attention recently, particularly with the success of SpaceShipOne in winning the Ansari X-Prize and the partnership announced between Scaled Composites and Virgin [1]. It reflects a growing trend in the development of the space tourism industry, a market identified with the potential to gross \$10 billion in the coming decades [2]. Although suborbital spaceflight is considered by most to be only an intermediate goal to opening up access to space, the development of these systems is critical for companies wishing to enter the space tourism market, especially in terms of fostering expertise and generating revenue.

However, suborbital spacecraft cannot just be thought of as reduced versions of their orbital counterparts; some issues can be considered in common,

although others will be distinct. As the majority of research in recent decades has focused on orbital and beyond spaceflight, it is necessary to ensure the assumptions made by work in these fields can be applied to suborbital conditions.

The Thunderstar capsule and its Starchaser 5 launch vehicle are currently under development at Starchaser Industries. The capsule can carry up to three crew to a maximum altitude of 150 km, during which time a number of manoeuvres need to be performed and for which an active attitude control system is required.

Control of attitude using quaternion feedback is an established concept [3–7]; however, most of the work has been based on orbital or deep space missions. Suborbital spacecraft present a unique problem because the timeframe for manoeuvres is many orders of magnitude smaller, requiring highly responsive control dynamics for large rotation angles. The intention of this case study is to develop an overall control architecture for the Thunderstar capsule, including the identification of suitable control laws and a top-level hardware specification. This is used to evaluate system feasibility and to highlight key

*Corresponding author: School of Mechanical, Aerospace and Civil Engineering, University of Manchester, PO Box 88, Manchester M60 1QD, UK. email: bill.crowther@man.ac.uk

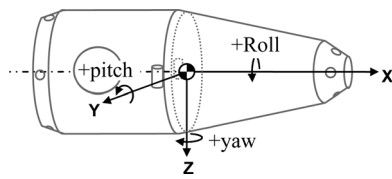


Fig. 1 Body axes coordinate frame for the Thunderstar spacecraft

considerations of applying such a system to a sub-orbital spacecraft.

1.1 Thunderstar attributes

The attitude of the Thunderstar will be controlled by a set of 12 nitrogen cold gas thrusters, arranged in opposing pairs to minimize any off-axis coupling. Excluding small perturbations to be discussed later, it has been assumed that the capsule is axisymmetric about its longitudinal *x*-axis. Figure 1 gives the body axes coordinate frame for the spacecraft, and Table 1 describes the basic attributes of the Thunderstar capsule.

1.2 Mission parameters

The Thunderstar capsule will be lifted to an altitude of around 100–150 km by a single stage rocket known as Starchaser 5. Once separated from the rocket and the launch escape system (LES), the active attitude control phase of the mission will begin. During this phase, it is required that the spacecraft undergoes a specific schedule of manoeuvres particular to the Thunderstar mission specification as depicted in Fig. 2. Relevant mission parameters are given in Table 2.

First, the capsule must stabilize itself following separation from the LES tower (phase I). Assuming a nominal mission scenario, the capsule is then required to roll about its longitudinal axis at a set rate (phases II and III). This is in order that the crew (passengers) get a good view of the Earth, moon, and other features through the portholes. This rotation will continue throughout the microgravity phase and has the

Table 1 Spacecraft parameters

Parameter	Value
Mass (m)	1400 kg
Roll inertia (J_{xx})	250 kg m ²
Pitch/Yaw inertia (J_{yy}/J_{zz})	970 kg m ²
Centre of gravity location (from capsule base) (X_{cg})	2.65 m
Capsule length (<i>X</i>)	3.70 m
Main body radius (<i>R</i>)	0.80 m
Cabin range from centre of gravity (<i>x</i>)	±0.85 m
Cabin radius from centre of gravity (<i>r</i>)	±0.70 m

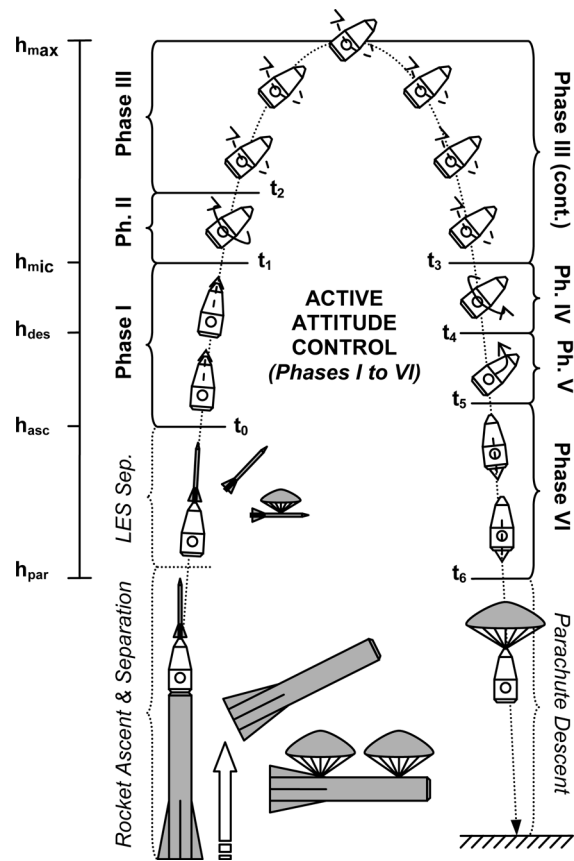


Fig. 2 Flight path and attitude dynamics over the active attitude control period

Table 2 Mission parameters

Parameter	Value
Separation velocity (u_0)	1.3 km s ⁻¹
Separation altitude (h_{asc})	70 km
Start of microgravity phase (h_{mic})	85 km
Apogee altitude (h_{max})	~150 km
Drogue chute deployment altitude (h_{par})	48 km
Required capsule rotation rate (<i>n</i>)	3 r/min
Time to acquire rotation rate (<i>n</i>) (t_n)	2 s
Duration of active attitude control (t_{06})	~5 min

secondary effect of giving some spin stabilization to the capsule.

As the capsule descends, it must reorientate itself into a nose-up vertical attitude and reduce the roll rate to zero in preparation for parachute deployment (phases IV and V). The magnitude of reorientation required is dependent on the dynamic pressure and the spin rate during phases I-III: due to the inherent aerodynamic directional stability of the capsule, high dynamic pressure, e.g. due to a low mission apogee, will tend to increase the angle through which the capsule must be reoriented. In contrast, increased spin rate will mitigate the effect of aerodynamic torques, and hence reduce the required reorientation angle.

The worst case is a reorientation angle of 180°. Note that de-spinning is critical to the safe operation of the capsule in order that the parachutes chords do not become tangled. Furthermore, during this time (phase VI), other attitude and rate deviations should be minimized. As the attitude control system is critical to the safe operation of the capsule, it is expected that its systems be at least singularly redundant.

At the end of the active attitude control phase, and prior to deployment of the primary parachute, it has been found from simulations performed in this work that a drogue chute should be deployed to provide further aerodynamic stability and increase capsule drag as it enters the denser atmosphere. The nominal altitude selected for this deployment is 48 km (based on the evaluation of the simulation presented in section 6.1). The primary parachute will be deployed at 30 km.

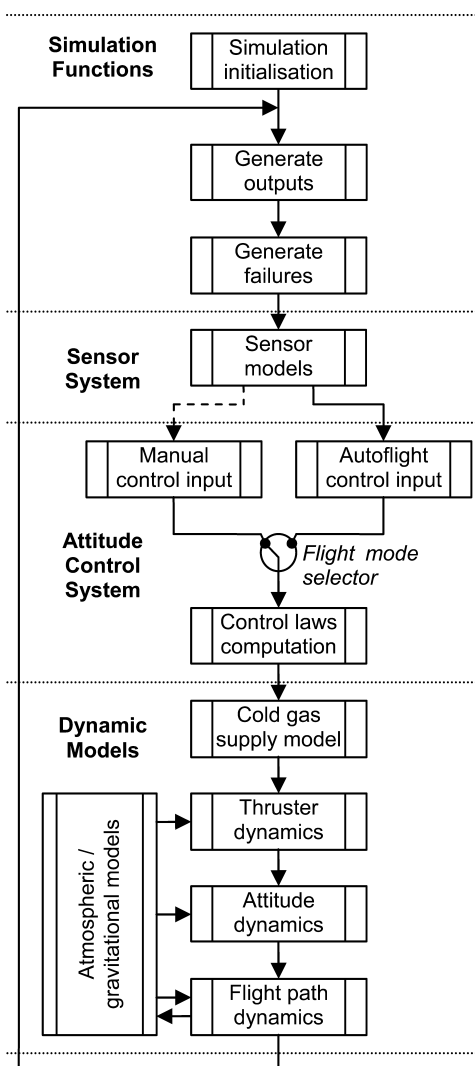


Fig. 3 Overview of the simulation processes

1.3 Simulation process

The definition of the simulation process is critical to the future development of the system model; it needs to be flexible and open to allow additional subsystems to be added and existing modules to be modified. Following a review of published simulation approaches, it was decided to adopt a modified and reduced version of the architecture proposed in reference [8]. A summary of the simulation processes required is shown in Fig. 3.

2 SPACECRAFT ATTITUDE DYNAMICS

2.1 Rigid body dynamics

Euler's equations for a spinning body written about the principal reference frame with $J_{yy} = J_{zz}$, and rearranged to make angular momentum the subject reduce to those given in equation (1). Note that the pitch and yaw rotations are coupled due to the inequality ($J_{xx} \neq J_{yy} = J_{zz}$) in the inertial matrix, \mathbf{J} . This will result in the motion about an axis even when no moment has been applied about that axis [9]. Note also that the torque vector, \mathbf{T} , includes both disturbance and control torques

$$\mathbf{J}\dot{\boldsymbol{\omega}} = \mathbf{T} - \begin{bmatrix} 0 \\ (J_{zz} - J_{xx})\omega_x\omega_z \\ (J_{xx} - J_{yy})\omega_x\omega_y \end{bmatrix} \quad (1)$$

Because of the rotational symmetry of the capsule, the aerodynamic forces and moments may be conveniently represented as functions of a single reference angle, namely the absolute incidence, σ , defined as

$$\cos \sigma = \hat{\mathbf{x}} \cdot \mathbf{V} = \cos \alpha \cos \beta \quad (2)$$

where $\hat{\mathbf{x}}$ is the unit vector in the body axis x , \mathbf{V} the capsule velocity vector, and α and β the angle of attack and sideslip, respectively.

2.2 Control torques

An actuation cycle for a generic cold gas thruster, based on linear simplifications adopted from reference [9], is shown in Fig. 4. The thruster torque profile reflects both the processing lags due to the controller and the lags due to the dynamics of the gas as it passes through the valve. The controller delays, t_{01} and t_{34} may be estimated with knowledge of the processing required and will be relatively small when compared with the fluid dynamic lags. For the present study, the controller lag was taken as 20 ms. On the basis of reference [10], the lags in the fluid dynamics producing the rise, t_{12} , and fall, t_{45} , times have been estimated as

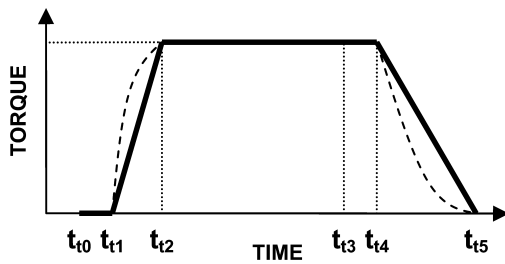


Fig. 4 Torque profile of a typical cold gas thruster (dashed line, typical performance; solid line, approximated)

120 and 300 ms, respectively. In actuality, the lag values will be a function of the delivered thrust design point of the device. Typically, this information would have to come from experiments on the actual flight hardware.

The maximum control thrust delivered by the thrusters can be made insensitive to the supply pressure by installing an appropriate step-down pressure regulator in the system. This allows a thrust schedule for a specific operation to be closely estimated prior to any manoeuvre. Equation (3) may be used to estimate the total maximum torque, T_{\max} , that may be required for manoeuvring about an axis of rotation. The acceleration limit, a_{lim} , has been defined based on the maximum rate and time to acquire rate mission parameters given in Table 2. The thrust factor, k_t , is a variable in the model and accounts for any disturbance effects (discussed in the next section) that could influence the spacecraft and must be positive and non-zero. For all the following work, the thrust factor has been set as 0.2. This is based on the assumption that the disturbance torques will be not greater than 20 per cent of the control for any significant time

$$T_{\max} = Ja_{\text{lim}}(1 + k_t) \quad (3)$$

Having calculated the maximum torque, the magnitudes of thrust required in each of the thrusters can be evaluated from the ratio of moment arms acting for a rotation in a positive and in a negative direction (Table 3). The total mass flow through the system is obtained using equation (4), where F is the summed thrust magnitudes from the 12 thrusters and I_{sp} the specific impulse of the gas measured at sea level. For the present work, the specific impulse for nitrogen cold gas is taken as 60 s based on data from reference [11]

$$\dot{m}_f = \frac{\sum |F_{1,\dots,12}|}{I_{\text{sp}}g_0} \quad (4)$$

Finally, the thrust impulse, maximum frequency, and minimum deliverable torque may be determined based on the system lags stated earlier, with a small

interval period, t_c , of 5 ms for control reversal within the processors. As the controller lags were assumed constant over all the thrusters, it follows that the maximum frequency, which is a function of their summation and given in equation (5), will be constant and is found to be around 20 Hz. The minimum deliverable torque from a single firing follows from the thrust impulse and is averaged over the minimum cycle time. Table 3 summarizes the findings from the analysis of the thrusters, noting that the direction of positive and negative torques are defined in Fig. 1.

$$f_{\max} = \frac{1}{t_{\text{cyc,min}}} = \frac{1}{t_{01} + t_{34} + 2t_{\text{rev}}} \quad (5)$$

Owing to the difficulties in aligning the roll thrusters with the longitudinal location of the centre of gravity, there are some secondary torques associated with them, indicated by the grey shading. As a percentage of the torque provided in the primary roll plane, the roll thrusters provide secondary torques equating to 10.5 and 2.6 per cent in pitch and yaw, respectively. Assuming normal operation, when both thrusters are fired at the same time, these will cancel out; however, in the event of a single failure, these secondary torques may not be ignored.

2.3 Disturbance torques

When modelling disturbances to the spacecraft attitude, both those internal and external to the system need to be considered. The disturbances internal to the capsule will alter the centre of gravity and inertia matrix of the spacecraft and could be caused by crew motion, hardware motion, or fuel slosh. With no large moving parts expected within the capsule, hardware motion should be negligible and so will not be considered further. Unlike most orbital missions, the fuel fraction aboard the capsule will be small, being no more than 0.01 by mass. As the tanks will also maintain a near constant pressure and be relatively low in volume ($<0.02 \text{ m}^3$), fuel slosh should be minimized and so will not be considered in the simulation.

Crew motion will be restricted to the microgravity phase when the occupants are free to move about the capsule. With reference to the capsule mass, it is expected that the crew mass fraction will be around 0.17. This is very high in comparison to other orbital and suborbital capsules. Although complex models for analysis of crew motion do exist, since the cabin is located at the centre of gravity and allows only restricted movement, it should be sufficient to simulate the effects through Brownian noise. The noise power is defined by assuming a crew of three, each capable of transferring an RMS-averaged force of 9 N [13] anywhere within the

Table 3 Thruster characteristics

Thruster		<i>s</i> (mm)	<i>F</i> (N)	Impulse (N/s)		Torque (Nm)				
				Rise	Fall	Roll	Pitch	Yaw	Min	
1	Positive roll	S'd	873	27.0	224.9	90.0	23.6	2.6	0.6	2.0
2	Negative roll	S'd	-873	27.0	224.9	90.0	-23.6	-2.6	0.6	-2.0
3	Positive pitch	Fore	2314	39.5	329.2	131.7	0.0	91.4	0.0	7.8
4	Negative pitch	Fore	-2314	39.5	329.2	131.7	0.0	-91.4	0.0	-7.8
5	Positive yaw	Fore	2314	39.5	329.2	131.7	0.0	0.0	91.4	7.8
6	Negative yaw	Fore	-2314	39.5	329.2	131.7	0.0	0.0	-91.4	-7.8
7	Positive roll	Port	873	27.0	224.9	90.0	-23.6	-2.6	-0.6	2.0
8	Negative roll	Port	-873	27.0	224.9	90.0	23.6	2.6	-0.6	-2.0
9	Positive pitch	Aft	1512	60.5	503.9	201.5	0.0	91.4	0.0	7.8
10	Negative pitch	Aft	-1512	60.5	503.9	201.5	0.0	-91.4	0.0	-7.8
11	Positive yaw	Aft	1512	60.5	503.9	201.5	0.0	0.0	91.4	7.8
12	Negative yaw	Aft	-1512	60.5	503.9	201.5	0.0	0.0	-91.4	-7.8

limits of the cabin range (Table 1). External torques from the environment could come from a number of sources: aerodynamics, the gravity gradient acting across the spacecraft, the Earth's magnetic field, or solar radiation. Reference [7] reports that the only disturbance torque of significance at altitudes <500 km is due to aerodynamics, although this work was primarily concerned with a spacecraft whose mission duration is 10^4 greater than the Thunderstar. Therefore, further analysis of the aerodynamic effects has been performed to establish its influence over this high-altitude, short-duration mission.

The aerodynamic forces and moments acting on the capsule may be modelled as a function of the absolute incidence (equation (2)), centre of pressure, and Mach number [13]. Values for the centre of pressure and normal force as a function of Mach number and absolute incidence were calculated using a method provided by ESDU [14] applied to a simplified capsule geometry. Axial force was estimated from data in reference [13]. Aerodynamic data were accessed by the simulation via a precomputed two-dimensional look-up table.

3 SPACECRAFT SYSTEM DEVELOPMENT

This section introduces the method of attitude guidance and control proposed by this case study. Key aspects of other subsystems are developed in order to establish their interaction with the primary system and so create a higher fidelity simulation. The subsystems considered are the sensor system used to provide feedback to the control laws, the thruster dynamics, and the propellant supply system used to deliver nitrogen to the thrusters.

3.1 Attitude guidance and control system

Numerous actuation methods for attitude control have been proposed and utilized on spacecraft, of which momentum devices and torque thrusters are the most common [11]. For the present application, the relatively high values of torque required during the reorientation manoeuvre leads to a significant mass penalty for momentum devices [11], leading to choice of torque thrusters as the preferred actuation method.

During the active attitude control phase of the mission (Fig. 2), the guidance system outputs values of spacecraft attitude and rate demand as a function of spacecraft position. The attitude control system then orientates the vehicle to meet the demanded values. The guidance system uses an Earth-fixed reference frame, whereas the attitude control system uses a body-fixed reference frame.

The control process essentially consists of finding the answers to two problems, one continuous and one discrete, within a feedback loop.

1. Given an attitude error or an angular rate error, how much torque demand is required to achieve the control objectives?
2. Given a torque demand, which thrusters should fire and for how long to achieve the control objectives to within a specified accuracy?

The first part of the problem has been solved using a generic quaternion attitude control technique developed by Wie and Barba [4]. As a method for describing attitude, quaternion representation offers significant advantages over Euler angles and other techniques. Quaternions exhibit no inherent singularities in geometrical orientation or differential rates, while still conforming to basic mathematical rules for addition and non-commutative multiplication [15, 16].

The second part of the problem is suited to the use of sliding mode theory [16–18], which is frequently used in thruster control systems; this has been implemented in the feedback loop using signal modulation. Sliding mode theory divides the state space of the system into discrete domains, where each thruster can be on or off. By arranging the thrusters into three sets, each aligned about a primary axis of rotation, the state space will now be divided into three discrete domains per set. With reference to Table 3, the three domains are: positive on, negative off; positive off, negative on; and all off. The positive on and negative on regions are defined by the switching line, which may be expanded to include the deadband, where all thrusters in a set are off; this has been implemented using a Schmitt trigger [11, 19]. The inclusion of a deadband ensures that the thrusters do not fire for small perturbations in angle or rate, thus wasting propellant. As the torque profile does not rise or fall instantaneously, the average torque, T_{avg} , will increase with the thruster cycle time, t_{cyc} , and will tend towards the maximum torque, T_{max} , as in equation (6) (times are defined in Fig. 4).

$$T_{avg} = T_{max} \left[1 - \frac{t_{t01} + 1/2(t_{t12} + t_{t45})}{t_{cyc}} \right] \quad (6)$$

3.2 Thruster and propellant supply systems

For this case study, a cold gas thruster and supply model that can be used for a number of purposes has been developed: to evaluate nitrogen usage, to examine the effect of system failure modes, and to generate instrumentation data for the purposes of crew training. Following a failure modes and effects analysis using this model, it was identified that a propellant leak from the thrusters could lead to a catastrophic failure. On this basis, a decision was made that the system should be at least a dual redundant, twin tank arrangement with a crossover feed. The proposed system is shown in Fig. 5, with the valves set for standard operation.

A thruster subsystem has also been developed as part of the spacecraft preliminary design and is shown in Fig. 6. It consists of the electromechanical and solenoid valves immediately before the thruster and its nozzle (all elements after the cock valves shown in Fig. 5).

To protect against a solenoid malfunction where a continuous flow of nitrogen emits from the nozzle, further control logic has been added to the electromechanical valve. With this closed loop system attached to the thrusters, uncontrolled firings may be prevented in milliseconds, rather than requiring the crew to react (leading to much higher angular rates). The logic ensures that if a pressure is measured above the threshold, indicating that the thruster is emitting nitrogen but a fire command has not been

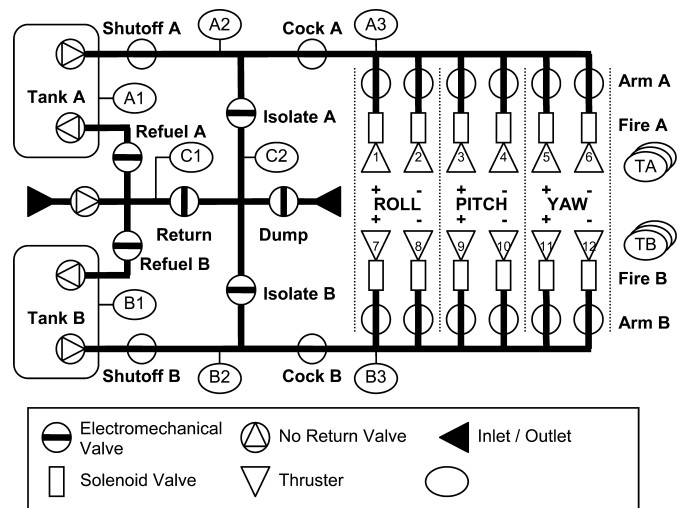


Fig. 5 Cold gas supply system architecture

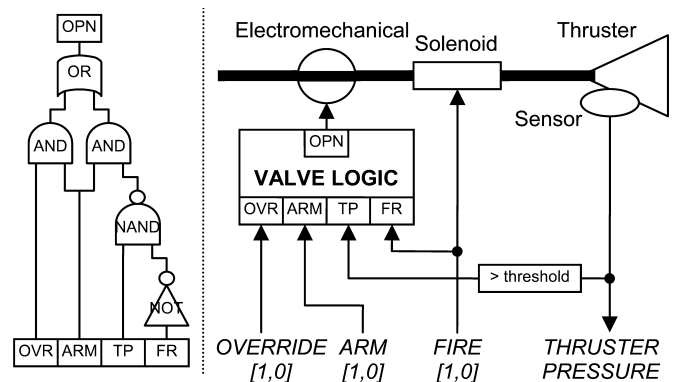


Fig. 6 Thruster subsystem architecture

received from the control laws, the electromechanical valve shuts. An override switch allows the crew to take over control of the valve should this system itself malfunction.

3.3 Attitude and altitude sensor system

The attitude sensor system for the spacecraft will primarily consist of dual-redundant laser ring rate gyros, which will be used to measure rates and integrated to find angles. On the basis of reference [11], the sample rate of the gyros is expected to be of the order of 25 Hz, with a drift of 2.0° h^{-1} and walk of $0.3^\circ \text{ h}^{-1/2}$. The initial pointing error has been estimated as 0.5° ; this is therefore the largest contributor to uncertainty in the attitude for the short duration of the active attitude control phase (~ 6 min). In order to maintain pointing accuracy over the mission, this will require connection to the Starchaser 5 sensor systems through an umbilical during the high-vibration environment of powered rocket flight.

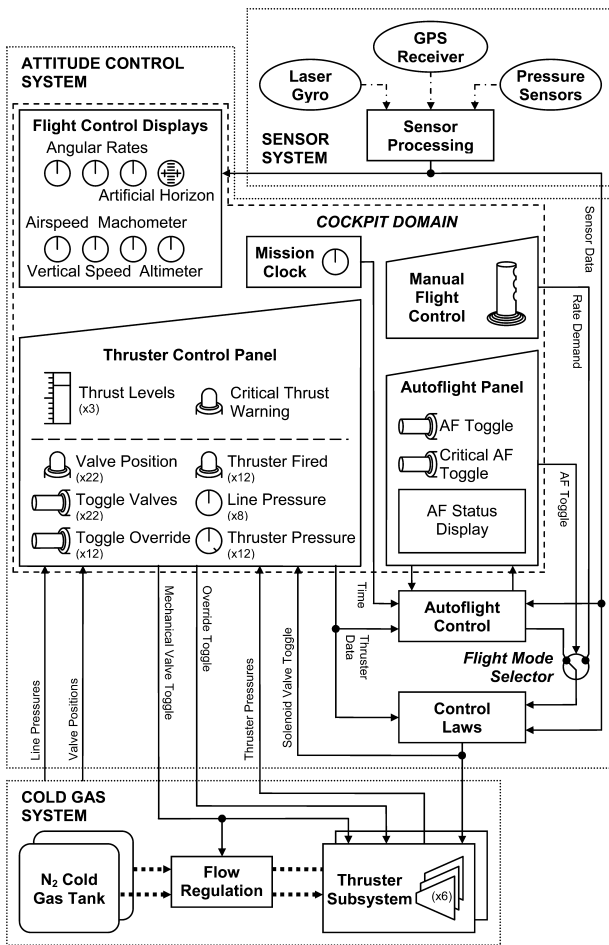


Fig. 7 Interactions within the attitude control systems

For altitude (and velocity), a global positioning system (GPS) receiver has been selected. For additional redundancy at low altitudes, static and dynamic pressure sensors will also be utilized. On the basis of tests performed on suborbital sounding rockets, it is expected that the GPS performance accuracy will be at least ± 2 km and ± 100 m/s [20].

3.4 System integration

The simulation process is intended to reflect the entirety of the Thunderstar system, initially encompassing those systems related to attitude control, but with the potential for expansion. Figure 7 shows the systems interactions that were considered in the initial development of the simulation; it covers the three systems outlined in section 3 and defines the cockpit interface required for manual flight control.

4 ATTITUDE GUIDANCE AND CONTROL SYSTEM

The control laws of the system are established in this section, with the gains and modulation characteristics

defined and related to the system specification. Although in off-nominal conditions manual control may be required, control through the autoflight is the primary mode of operation for the Thunderstar capsule. Consequently, this section focuses on the autoflight and the generation of a schedule of demands for the control laws, rather than considering frequency responses and human factors of the system. Finally, the limitations in the laws are discussed, and methods to compensate for this by updating the control laws are suggested.

4.1 Control law development

Equations (7a to c) give the three sets of control laws proposed in reference [4] for setting the demand torque, T_d . The control laws have been modified such that the command torque and rate gains appear in diagonal matrices; this will prove useful in later analysis. The control laws have a single quaternion gain, K_0 , and a diagonal matrix of three rate gains, \mathbf{K} , to be defined

$$T_d = -T_c [K_0 q_{13} + K\omega] \tag{7a}$$

$$T_d = -T_c \left[\frac{K_0}{q_0^3} q_{13} + K\omega \right] \tag{7b}$$

$$T_d = -T_c [\text{sign}(q_0) K_0 q_{13} + K\omega] \tag{7c}$$

with

$$T_c = \text{diag} [T_{\max}] = \begin{bmatrix} T_{xx,\max} & 0 & 0 \\ 0 & T_{yy,\max} & 0 \\ 0 & 0 & T_{zz,\max} \end{bmatrix}$$

$$K = \begin{bmatrix} K_{xx} & 0 & 0 \\ 0 & K_{yy} & 0 \\ 0 & 0 & K_{zz} \end{bmatrix}$$

It was found that equation (7c) provided the most robust solution at any initial orientation without the possibility of an infinite control signal, although all would be suitable for inclusion if required. The key differences in the responses of the control laws lie with two performance criteria. First, when the Euler angle error approaches 180° (implying $q_0 \rightarrow 0$), and secondly, when an orientation of $>180^\circ$ is demanded (implying $q_0 < 0$). If $q_0 = 0$, it is possible that the gain in equation (7b) can become infinite, although in doing so, it does allow a more flexible control compared to equation (7a), which ignores the value of q_0 , and hence the required direction of rotation. Equation (7c) is a composite of the two preceding laws, therefore providing: ‘an efficient reorientation manoeuvre for an arbitrary initial orientation without the possibility of an infinite signal’ [4]. In its present

form, the control law will suffer from a number of limitations if implemented into the Thunderstar, which needed to be addressed by the present work.

1. The control law assumes instantaneous (infinite jerk) thruster profiles; the actual cold gas thrusters will have much more variance in the possible control torques with respect to the maximum. As has been shown in equation (6), the average torque only tends towards the maximum; if the cycle time is low, the total impulse will also be significantly lower than that assumed by the control law.
2. The control law assumes that each thruster set acts only within a single control plane; this is true for the thrusters to be employed on the spacecraft, except in roll following a single failure. In this case, roll demands will cause moments about all planes and could lead to excessive propellant use.
3. The control law does not allow angular rate demands; for the present work, this is a requirement for the roll axis in autoflight and during manual control.

Assuming a thruster period resulting in a frequency not lower than 1 Hz, and including rise and decay responses, the effective torque range is between 8 and 75 per cent of the maximum, T_{\max} . For attitude hold manoeuvres, a high torque is not required and therefore a lower control torque could be imposed in the control laws, saving propellant reserves at the expense of reduced peak acceleration [17]. When a large orientation or rate is required, then the system can be programmed to switch to a higher magnitude control torque. In the current implementation, the switch is operated by the autoflight, as the manual flight control is assumed to be fixed rate (and hence fixed mode). Through numerical analysis of the mode factor with respect to the maximum torque and the resultant acceleration and rate, the control torque was set with a mode factor of $MF_{\text{low}} = 0.4$ and $MF_{\text{high}} = 1.0$ for low and high modes, respectively.

Failure compensation in the control laws can be implemented by making use of the control torque matrix introduced earlier. In the no-failure case, the matrix would remain diagonal, but if a thruster failure results in a cross-torque, it can be modified to prevent instability (cross-torque is only applicable to the failure of a roll thruster in this spacecraft; Table 2). By including the negated values of these secondary torque terms, it follows that every time a roll demand that results in secondary torques is made, the control system can be induced to fire pitch and/or yaw thrusters to compensate as necessary. This is shown in the updated control torque calculation in equation (8), which also includes the mode factor. Obviously, it is required that the compensation is only applied when the torque demand is of the same sign

as the cross-torquing thruster (i.e. the thrusters causing the cross-torque will fire) and so some logic, such as that outlined in equation (9), is required

$$\mathbf{T}_c = MF \begin{bmatrix} T_{xx,\max} & 0 & 0 \\ T_{yx} & T_{yy,\max} & 0 \\ T_{zx} & 0 & T_{zz,\max} \end{bmatrix} \quad \text{with} \quad (8)$$

$$T_{yx} = -T_{i,y}a \quad T_{zx} = -T_{i,z}a \quad (8)$$

$$a = \left| \frac{\text{sign}[T_{i,x}] - \text{sign}[\text{sign}[q_d]K_0q_1 + K_{xx}\omega_x]}{2} \right| \quad (9)$$

The implementation of a torque demand from rate is relatively simple, as the pulse-width pulse-frequency (PWPF) modulator, discussed next, can filter any excessive or low torque demands. By analysing the measured angular rate compared with the demanded one in the autoflight, integrating the result, and then transforming into quaternions, an effective rate demand can be synthesized, as in equation (10)

$$\mathbf{q}_d = \int f(\omega_d - \hat{\omega}) \cdot ds \quad (10)$$

4.2 Control law gains

It is generally found that the gains in an (orbital) spacecraft proportional derivative controller should be set as in equation (11) [21]; from the present work, it has been found that these are also suitable values for the suborbital control system considered here. Although not implemented in the present work, it would be possible to generate modified gains for the failure cases. This would be particularly useful if the cross-torques represented a significant proportion of the maximum torque, which would occur if there was greater misalignment of the thrusters with respect to the principal axes

$$K_0 \approx 2\omega_n^2 \mathbf{J} \mathbf{T}_c^{-1} \quad (11a)$$

$$\mathbf{K} \approx 2\zeta \omega_n \mathbf{J} \mathbf{T}_c^{-1} \quad (11b)$$

For the present case study, a critically damped response has been selected, i.e. $\zeta = 1.0$, based on the recommendations of reference [19]. With a constant damping term, the time response of the system will be dependent on the closed-loop natural frequency, ω_n . Selecting a system with a low-natural frequency ($\omega_n < 1/2\pi$ rad) ensures the control system is stable [11]. Figure 8 shows the number of thruster firings (an indication of stability, as the system should be seeking to attain a steady state where no firings are required) against the closed loop natural frequency; a value of $\omega_n = 1/4\pi$ rad was used in the simulation (marked 'x' on the plot).

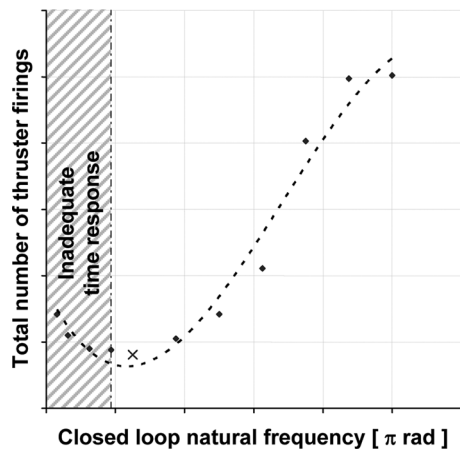


Fig. 8 Relationship between number of thrusters firings and closed loop natural frequency

4.3 Pulse-width pulse-frequency modulation

Taking the modulator gain to be at unity, i.e. $K_m = 1$, and the Schmitt trigger output equal to the maximum torque, $U_m = T_{max}$, the equations for the time behaviour of a PWPF modulator can be simplified from those described by Sidi [11], giving those in equations (12a and b)

$$t_{on} = -\tau_m \ln \left(1 - \frac{H}{T_{max} - T_d + U_{on}} \right) \tag{12a}$$

$$t_{off} = -\tau_m \ln \left(1 - \frac{H}{T_d - U_{off}} \right) \tag{12b}$$

with

$$H = U_{on} - U_{off}$$

The modulator behaviour now depends on three variables: the time constant, τ_m , and its on and off thresholds, U_{on} and U_{off} . The on and off thresholds correspond to the deadband required, which can be partially determined by looking at the characteristics of the thruster, remembering that it is undesirable for the modulator to be triggered for a torque demand that is lower than is possible from the thrusters. As has already been shown, the minimum on-time, $t_{on} = 25$ ms (for a maximum thruster frequency of 20 Hz), results in a minimum torque for each thruster (Table 3). The modulator on threshold should therefore be applicable at the minimum torque possible and multiplied by a scaling factor, E , in order to prevent valve chatter in the presence of any sensor noise or other perturbations (equation (13)). Previous work [17] recommends that $E = 0.1$ is suitable

$$U_{on} = T_{d,min} = (1 + E)T_{min} \tag{13}$$

Including lags and decay times, the total cycle time is 108 ms for $t_{on} = 25$ ms; therefore, the time off

behaviour must be limited by the inequality stated in equation (14)

$$t_{off} \geq t_{cyc} - t_{on} \tag{14}$$

By rearranging equation (12a) to make U_{off} the subject allows for the exploration of its relationship to τ_m , remembering that the time constant must be a real positive number. From the analysis of this relationship, a time constant of $\tau_m = 0.5$ has been selected for the trigger, satisfying the condition of equation (14), while minimizing the phase lag.

4.4 Autoflight scheduling

The autoflight needs to control two variables in the spacecraft attitude; these are its roll rate, $\dot{\phi}$, and absolute incidence, σ , which itself is a function of the sideslip and angle of attack, and are both measurable by the system. In terms of the active attitude control phases (originally defined in Fig. 1), Table 4 summarizes the required changes in these two variables.

Phases V and VI, immediately prior to parachute deployment, will be the most critical for the safe return of the capsule. During this time, the capsule is not gyrostabilized and so could suffer from instability. It is therefore desirable that these phases be as rapid as is possible without compromising safety margins.

It is undesirable for control systems to have large steps in demand; for example, this would be the case if, in phase II, the autoflight stepped the roll rate demand from zero instantaneously. It is more preferable to input the step change gradually, which can be done using equations (15) (for an angle and a rate demand, respectively); this gives the acquire time for a specified demand

$$t_{acq} = \left(\frac{\omega_{lim}}{\alpha_{lim}} + \frac{\theta_d}{\omega_{lim}} \right) + t_{t01} \tag{15a}$$

$$t_{acq} = \left(\frac{\omega_d}{\alpha_{lim}} \right) + t_{t01} \tag{15b}$$

A further modification to extend the modes of autoflight operation could be made to include some intermediate functions, such as specific acquire and hold modes for rates and angles in roll, pitch and yaw, and angle of attack. This change would be simple to

Table 4 Autoflight demand parameters

Autoflight mode	$\dot{\phi}$ (rad)	σ (rad)
I Hold absolute incidence	0	0
II Acquire roll rate	$0 \rightarrow \dot{\phi}_d$	Undefined
III Hold roll rate	$\dot{\phi}_d$	Undefined
IV Acquire roll rate	$\dot{\phi}_d \rightarrow 0$	Undefined
V Acquire absolute incidence	0	$\sigma_{des} \rightarrow \pi$
VI Hold absolute incidence	0	π

implement but will not be discussed further as the problem of guiding the spacecraft through a set of specific manoeuvres presents more of a control challenge for the system.

5 SIMULATION AND MODELLING

This section describes the practical implementation of the preceding work into a SIMULINK model. Plots of the primary data from the simulation are presented in order to evaluate the performance of the attitude control concept for a suborbital mission.

5.1 SIMULINK model architecture

Figure 9 gives an overview of the ‘spacecraft attitude, guidance, and control’ block implemented in the SIMULINK model. It receives altitude and aerodynamic torque signals from the ‘flight path dynamics’ block and returns the attitude and angular rate of the spacecraft. The ‘autoflight computer’ block uses a schedule developed prior to the simulation from the mapped flight path and the maximum acceleration and rates acceptable. When a rate or angle is unspecified for a particular phase in the flight, such as the roll angle during the reorientation manoeuvre, the demand is synthesized from the measured rate. The block also calculates the normal to the absolute incidence plane, and hence the axis about which the reorientation of the spacecraft takes place.

The ‘cold gas supply model’ block was simplified from the design shown in Fig. 6 by excluding the refuel and return valves. This is because no refuelling can

take place in the period considered by the simulation; however, it also means that the fuel transfer function of the valves is not included in the model.

5.2 Environmental models

Both atmospheric and gravitational models are required to simulate the environment in which the capsule moves. The WGS84 gravity model was selected, although accuracy is limited above 20 km and when the exact date is not defined. The latitude for launch has been set to be 30.925°, equivalent to that of the Woomera launch site 2 in Australia. The atmosphere has been modelled using the COESA extensions to the US atmosphere model, extending the data range up to 85 km and providing extrapolation for extensions beyond. Wind shear and gusts were not included in the atmosphere model since their effects are likely to be small and there are limited data available for high altitudes.

6 EVALUATION

6.1 Simulation results

The control system performance was initially evaluated for the nominal mission as described in section 1.2. Subsequently, a Monte-Carlo analysis was conducted in order to evaluate the robustness of the approach with respect to uncertainty in mission and system parameters. For parameters relating to the launch performance such as the separation altitude and initial velocity, a variance of ±10 per cent was

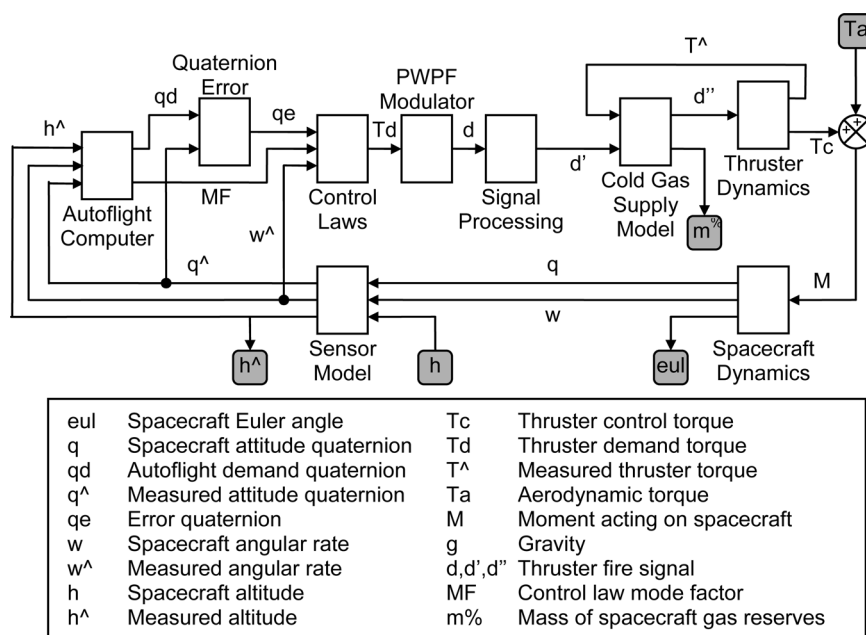


Fig. 9 Spacecraft attitude dynamics, guidance, and control block

considered. For parameters relating to the inertial properties of the spacecraft, such as centre of mass and inertia, these may be more tightly controlled prior to launch and so only a variance of ± 5 per cent was implemented. Variations in the performance of, and demand on, the thrusters were not included. Results for the nominal mission simulation are shown in Figs 10(a) to (d). Results of the Monte-Carlo analysis are shown in Fig. 11.

Figure 10(a) shows the roll rate demand and response over the entire mission. The spacecraft control system is able to quickly acquire and maintain a roll rate in the microgravity phase of the flight, and subsequently reduce this rate to zero during the spin-down phase prior to parachute deployment.

Figures 10(b) and (c) show the spin-up and spin-down phases of the mission in more detail, also including the roll thruster firing signals. In both figures, it may be seen that the signal to fire the thrusters is given after a lag of the order of 2 s. This is a result of implementation of the efficiency constraint by which the thruster control system filters out high-frequency control inputs and helps to avoid fuel waste from oscillating demands. After the initial delay, the response is approximately first-order with a time constant of around 4 s. There is some steady-state error due to the discrete nature of the thrusters; however, the magnitude is sufficiently small that there would be little payback from implementation of an integral term in the controller. Figure 10(d) gives the

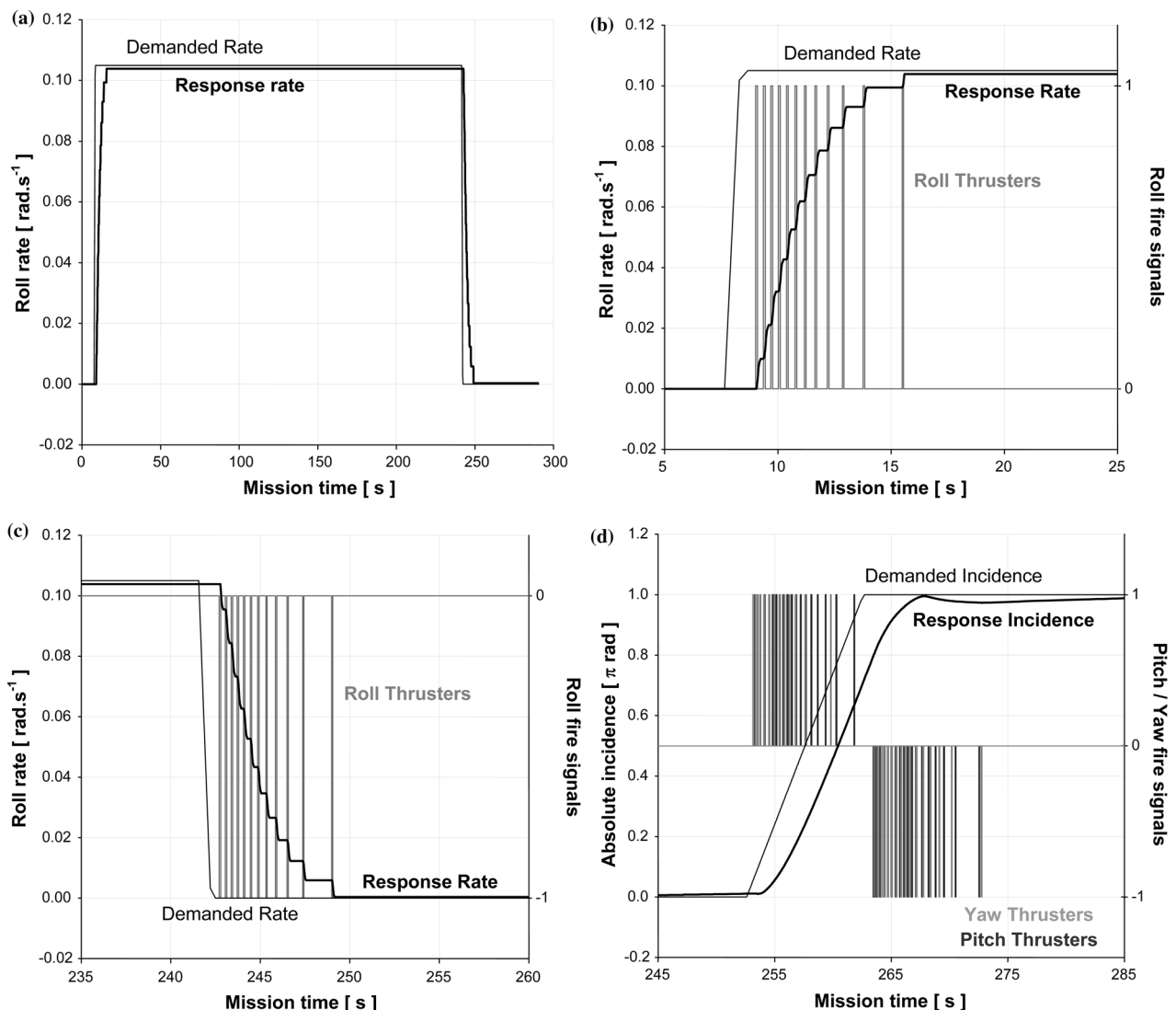


Fig. 10 Typical demands and responses for a nominal mission over the active attitude control period. (a) Roll rate demand and response over entire active attitude control period. (b) Roll rate demand, response, and roll thruster signals during spin-up. (c) Roll rate demand, response, and roll thruster signals during spin-down. (d) Absolute incidence, response, and pitch and yaw thruster signals during the reorientation manoeuvre

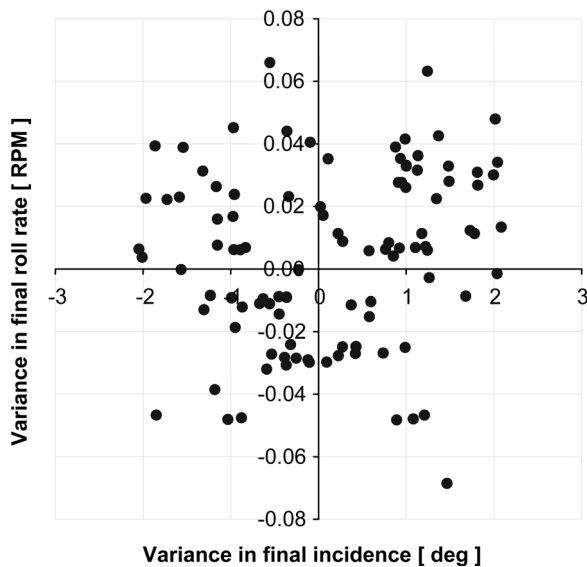


Fig. 11 Demonstration of control system robustness: variance of final roll rate and incidence due to random variation in mission and spacecraft parameters

absolute incidence angle demanded by the autoflight and the response for the reorientation manoeuvre, as well as the fire signals sent to the pitch and yaw thrusters over this period. Again, the control system is able to respond well to the demands. The response lags the demand by approximately 2 s for reasons outlined above, and the final error is approximately 3° ; this is acceptable in the reorientation, as drogue chute deployment will help stabilize the capsule further, minimizing small angle deviations in pitch and yaw.

Figure 11 gives the deviations in the demand and response roll rate and absolute incidence at the end of the active attitude control phase of the mission for 100 runs of the simulation under the variances stated previously. As may be seen in the plot, the maximum reorientation error is not more than 4° , and the maximum residual roll rate is not more than 0.08 r/min. This provides evidence that the control system approach is robust with respect to real-world uncertainty.

Analysis of the multiple simulation cases showed that the maximum amount of nitrogen propellant expended over the active attitude control phase was up to 7 per cent of the available load. It may therefore be possible to reduce the amount of nitrogen carried by the spacecraft, although this should be done after consideration of off-nominal mission scenarios, failures, and the need to maintain a near-constant pressure in the propellant tanks.

6.2 Simulation development issues

1. During the descent phase when the capsule enters the lower denser atmosphere, it was noted that the capsule experiences some low-amplitude high-frequency oscillations about an axis normal to the velocity vector. This has been attributed to yaw-roll lock-in and becomes significant when the dynamic pressure increases to >19 kPa, equating to an altitude of ~ 31 km in the flight profile (with neither of the parachutes assumed deployed). The oscillations increase to such an extent that thruster attitude control becomes inadequate at >100 kPa, equivalent to ~ 22 km altitude. Although the capsule control system is capable of providing enough thrust to compensate for this instability down to the primary parachute deployment altitude, the use of a drogue chute to further stabilize the capsule and reduce the amount of active control as it re-enters the denser atmosphere is recommended by this work.
2. Analysis of capsule accelerations on human factors needs to be considered in more detail for future work. Initial estimates suggest that during both drogue and main parachute deployment the peak longitudinal accelerations are around 7 g. It is recognized that this is high for a tourist flight and efforts may be needed to reduce this. The lateral acceleration due to the reorientation manoeuvre is approximately two orders of magnitude smaller and may be neglected.
3. The rise and decay times in the cold gas thruster give a much greater range of torques when compared with combustible thrusters such as hydrazine [7]. This has some advantages in that finer tracking is possible, but causes problems in the PWPF modulator which assumes that the thrusters are either on or off. It has been found that control of the capsule may be improved by modifying the modulator output, U_m , to be a fraction of the maximum torque rather than be equal to it, thus reflecting that the average torque provided by the thruster only tends towards maximum as the frequency tends to zero. A value of 0.6 has been found to produce good response in the system.

7 CONCLUSIONS

From analysis of the attitude control simulation, it has been shown that a successful version of the control laws defined by Wie and Barba [4] has been implemented for the control of a suborbital spacecraft. The interaction between these laws and an autoflight computer, with a schedule defining roll rate and absolute incidence to generate quaternion demands, has also been shown. The use of a PWPF modulator

to synthesize command signals to the thruster has been implemented and a process to define the system deadband is given. It is therefore concluded that by using the methods described in this paper it is possible to produce an automated guidance and control system to work under the conditions specified. Further work considering failures of system components and manual flight control is required before refinement of the control gains. In any review of the control system, consideration of the human factors is also required particularly in terms of the g -forces experienced by the crew.

The differences between the spacecraft discussed in this paper and previous orbital and suborbital capsules provided interesting design challenges. The control system response has been proved such that the mission profile is met over a very short active attitude control period (~ 5 min). The high rise and fall lags in the thruster profile have been overcome through the use of an additional variable to describe the modulator output U_m , based on the estimated fraction of maximum torque generated by the thrusters. The work has shown that the only significant internal disturbance is that caused by the movement of the crew in the capsule and the only external disturbance is the aerodynamic effects.

REFERENCES

- Dorheim, M. A.** SpaceShipOne wins the Ansari X-Prize. *Aviat. Week Space Technol.*, October 2004, 30–35.
- Space tourism market study, *Futron Corporation Market Report*. Available from <http://www.futron.com/...spacetourism> (cited May 2005).
- Crassidis, J. L., Markley, F. L., Antony, T. C., and Andrews, S. F.** Nonlinear predictive control of spacecraft. *AIAA J. Guid. Control Dyn.*, 1997, **20**(6), 1096–1103.
- Wie, B. and Barba, P. M.** Quaternion feedback for spacecraft large angle maneuvers. *AIAA J. Guid.*, 1984, **8**(3), 360–365.
- Wie, B.** Solar sail attitude control and dynamics. *J. Guid. Control Dyn.*, 2004, **27**(4), 526–535.
- Kim, Y. and Mesbahi, M.** Quadratically constrained attitude control via semidefinite programming. *IEEE Trans. Automat. Control*, 2004, **49**(5), 731–735.
- Wertz, J. R.** (Ed.) *Spacecraft attitude determination and control*, 1978, pp. 556–580 and 758–759 (Kluwer Academic Publishers, London).
- Norlin, K.** Flight simulation software at NASA dryden flight research centre. NASA-TM-104315, 1995.
- Hughes, P. C.** *Spacecraft attitude dynamics*, 1986, Chapters 4 and 8 (John Wiley & Sons, New York).
- Werking, R. D., Berg, R., Brokke, K., Hattox, T., Lerner, G., Stewart, D., and Williams, R.** *Radio astronomy explorer-B postlaunch attitude operations analysis*, NASA-X-581-74-227, 1974 (cited in reference 8).
- Sidi, M.** *Spacecraft dynamics and control*, 1997, Chapter 9 (Princeton University Press, London).
- Newman, D. J., Amir, A. R., and Beck, S. M.** Astronaut induced disturbances to the microgravity environment of the Mir space station. *J. Spacecraft Rockets*, 2001, **38**(4), 578–583.
- Barrowman, J. S.** The practical calculation of the aerodynamic characteristics of slender finned vehicles. NASA-TM-2001-209983, 1967.
- Computer program for the calculation of normal force and pitching moment of forebody-cylinder combinations at angles of attack up to 90° and mach numbers up to 5, including the effects of conical boat-tailing. ESDU paper 90034, 1995.
- Kuipers, J. B.** *Quaternions and rotation sequences*, 2002, Chapters 4–6 and 10 (Princeton University Press, Oxford).
- Walchko, K. J.** Robust nonlinear attitude control with disturbance compensation, University of Florida, 2003, available from http://etd.fcla.edu/UF/UFE0000818/walchko_k.pdf (cited March 2005).
- Foley, J. D.** Control of a spacecraft using a reaction control system. In Proceedings of the 20th Annual Summer Computer Simulation Conference, Seattle, 1988, pp. 236–240.
- Wie, B. and Plescia, C. T.** Attitude stabilization of flexible spacecraft during stationkeeping maneuvers. *AIAA J. Guid.*, 1984, **7**(5), 430–436.
- Kaplan, M. H.** *Modern spacecraft dynamics and control*, 1976, Chapters 4–6, p. 246 (John Wiley & Sons, New York).
- Markgraf, M., Montenbruck, O., and Leung, S.** A flexible GPS tracking system for suborbital and space vehicles. 9th St Petersburg International Conference on *Integrated navigation systems*, St. Petersburg, 27–29 May 2002.
- Wie, B.** *Dynamic modelling and attitude control of solar sail spacecraft*. Contract report number 1228156, NASA Solar Sail Technology Working Group, 2002, pp. 33–35.

APPENDIX

Notation

a, a_{lim}	angular acceleration and limit
E	valve noise attenuation factor
F	thrust (applied force)
g_0	gravity at sea level
I_{sp}	cold gas specific impulse
J	inertia tensor
k_T	thruster sizing factor
K_0, K	quaternion scalar gain and rate gain
m_f	mass of cold gas propellant
MF	thruster mode factor
q_0, \mathbf{q}_{13}	quaternion: scalar part, vector part
\mathbf{q}_d	demand quaternion
\mathbf{q}_e	error quaternion
Q	jerk (dT/dt)
s	thruster moment arm
t, t_{acq}	mission time and acquire time
t_f, t_{cyc}	thruster fire and cycle times
$t_{\text{on}}, t_{\text{off}}$	modulated on and off times
T	torque

T_c	Control torque	ζ	damping ratio
T_d	demand torque	θ_d	demand angle
U_{on}, U_{off}	modulator on and off thresholds	σ	absolute incidence
U_m	modulator output	τ_m	modulator time constant
		ω_n	natural frequency
α	angle of attack	ω, ω_{lim}	angular velocity and limit
β	sideslip	ω_d	demand angular velocity